Springer

KSME

Journal of Mechanical Science and Technology 30 (11) (2016) 5083~5091
www.springerlink.com/content/1738-494x(Print)/1976-3824(Online)
DOI 10.1007/s12206-016-1026-4

Stress recovery techniques for natural element method in 2-D solid mechanics †

Jin-Rae Cho*

Department of Naval Architecture and Ocean Engineering, Hongik University, Sejong 339-701, Korea

(Manuscript Received October 19, 2015; Revised May 22, 2016; Accepted June 8, 2016)

Abstract

This paper is concerned with the stress recovery for the natural element method in which the problem domain is discretized with Delaunay triangles and the structural behavior is approximated with Laplace interpolation functions. Basically, the global and local patch recovery techniques based on the L_2-projection method are adopted. For the local patch recovery, the local element patches are defined by the supports of each Laplace interpolation function. For the comparison purpose, the local stress recovery is also performed using Lagrange-type basis functions that are used for 3- and 6-node triangular elements. The stresses that are recovered by the present global and local recovery techniques are compared each other and compared with the available analytic solution, in terms of their spatial distributions and the convergence rates. As well, the dependence of the recovered stress field on the type of test basis functions that are used forbnov-Galerkin (BG) and Petrov-Galerkin (PG) natural element methods is also investigated.

Keywords: Natural element method; Stress recovery techniques; PG-NE method; BG-NE method; Laplace interpolation functions; Smoothened stress field; Global and local patches; Convergence rate

1. Introduction

The interpolation functions used in the symmetric Galerkin approximation should be square-integrable in order for the approximated behavior of continuum body to produce finite strain energy. Owing to this requirement on the interpolation function, both the trial and test functions in finite element methods should possess at least the C^0-continuity. But, it is well known that the C^0-continuity results in the approximate solutions in which strain and stress fields are discontinuous across the element interfaces. The occurrence of discontinuity in strain and stress fields not only deteriorates the numerical accuracy but also violates the physical constraint in continuum mechanics. In other words, strains and stresses as well as displacement in a continuum body should be continuous as far as the body is not broken out. Hence, the post-processing of the bare strains and stresses that were approximated using C^0-finite elements has been an inevitable job to obtain the acceptable continuous ones.

A simple stress recovery method is to obtain the globally continuous stress distribution by interpolating the stress values at Gauss integration points. It is of course based on the fact that the weighted residual approximation exhibits the superconvergence at the integration points [1]. In two- and three-dimensional finite element meshes, this simple concept for stress recovery is implemented by interpolating the nodal stress values using the stress values at Gauss integration points and by averaging the interpolated nodal stress values within a common element patch. In 1971, Brauchli and Oden [2] introduced a global stress recovery technique based on the L_2-projection method to obtain more accurate stress field which is continuous across the element interfaces. In 1992, Zienkiewicz and Zhu [3] introduced the Superconvergent patch recovery technique (SPR), for which the local element patches are constructed and the stress recovery is performed patch by patch to obtain the smoothened more accurate continuous stress field. Later, Blacker and Belytschko [4] also enhanced the superconvergent patch recovery technique by adding the squares of residuals of the equilibrium equation and the natural boundary conditions. Boroomand and Zienkiewicz [5] proposed an improved patch recovery technique, called the recovery in equilibrium (REP), in which the recovered stresses are equilibrated in the patch.

Meanwhile, the meshfree methods have been in the spotlight by many investigators since the early 1990s, as an alternative approximation method to overcome the inherent drawbacks of finite element method such as the preservation of element connectivity and the numerical quality deterioration stemming from the excessive element distortion. The representative meshfree methods are the Element free Galerkin method (EFGM) [6], the Reproducing kernel particle method (RKPM) [7], the h-p clouds [8], the Partition of unit method (PUM) [9] and the Meshless local Petrov-Galerkin (MLPG)

*Corresponding author. Tel.: +82 44 860 2546, Fax.: +82 41 862 0940
E-mail address: jrcho@hongik.ac.kr
† Recommended by Associate Editor Gang-Won Jang

[10] method. These methods surely provide the highly smooth approximate solutions, but at the same time those suffer from the common difficulties in the essential boundary condition enforcement and the numerical integration. Differing from these grid-point based meshfree methods, the Natural element method (NEM) introduced originally by Braun and Sambridge [11] uses the basis functions called Laplace interpolation functions which not only exhibit the high smoothness but also satisfy the Kronecker delta property [12, 13].

Thanks to the Kronecker delta property of Laplace interpolation functions and the introduction of Delaunay triangulation for defining Laplace interpolation functions, the natural element method does not require extra effort for imposing the essential boundary condition and employing the traditional Gauss quadrature rule for the numerical integration [14, 15]. Because of these merits, this method has been rapidly extended to solve the important engineering problems in linear and nonlinear solid mechanics by subsequent researchers [16-20]. As is illustrated in Refs. [12, 21], it has been justified that the Laplace interpolation functions possess the sufficiently smooth C^1-interpolant characteristic to overcome shear locking without the need of extra numerical technique. Nevertheless, whether or not such a prominent feature of Laplace interpolation functions does also appear at the level of strain and stress fields has not been sufficiently investigated. In other words, it has not been fully justified whether the natural element approximation leads to the acceptable accurate and smooth bare stress distribution without employing the stress recovery. Furthermore, it is questionable whether and how much the bare stress distribution could be improved by the stress recovery.

In this context, this paper is concerned with the stress recovery techniques for the natural element method in 2-D linear elasticity. Basically, the L_2 projection-based global and local stress recovery techniques [2, 3] using Laplace interpolation functions are adopted. The stress recovery itself may be thought of an old subject tracing back to the late 1990s. But, most studies on the natural element method focused on the application to major engineering problems so that the stress recovery has been rarely studied. In this regard, this subject is worthwhile and laid the basis for more advanced research subjects such as the error estimation and the adaptivity.

For the local stress recovery, the supports of each Laplace interpolation function serve as individual local element patches. As well, for the comparison purpose, the local stress recovery is also performed using Lagrange-type basis functions for 3- and 6-node triangular elements, for which each local element patch is constructed according to Zienkiewicz and Zhu [3]. The presented stress recovery techniques are evaluated by comparing each other and by comparing with the existing analytic solution, in terms of the stress distributions and the convergence rates to the total number of grid points. Furthermore, the dependence of the recovered stress field on the type of test basis functions used for the natural element approximation, that is the difference in the recovered stress fields between Bubnov-Galerkin (BG-NEM) and Petrov-Galerkin natural element methods (PG-NEM), is also investigated.

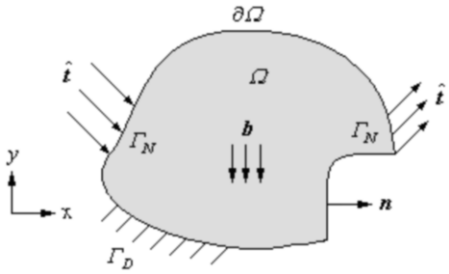

Fig. 1. A 2-D linear elastic body under small deformation.

2. Natural element approximation of 2-D linear elasticity problem

Let us consider a 2-D linear elastic body shown in Fig. 1 which occupies an open bounded domain $\Omega \in \Re^2$ with the boundary $\partial\Omega = \overline{\Gamma_D \cup \Gamma_N}$, where Γ_D is the displacement boundary while Γ_N denotes the traction boundary. Assuming the small deformation, the displacement field $\mathbf{u}(\mathbf{x})$ is governed by the static equilibrium given by

$$\nabla \cdot \sigma + \mathbf{b} = 0 \quad in \quad \Omega \tag{1}$$

with the displacement and traction boundary conditions:

$$\mathbf{u} = \hat{\mathbf{u}} \quad on \quad \Gamma_D \tag{2}$$

$$\sigma \cdot \mathbf{n} = \hat{\mathbf{t}} \quad on \quad \Gamma_N . \tag{3}$$

In which σ indicates the Cauchy stress, $\mathbf{b}$ the body force, $\mathbf{n}$ the outward unit vector normal to $\partial\Omega$ and $\hat{\mathbf{t}}$ the surface traction.

The virtual work principle converts the boundary value problem Eq. (1) to the weak form: Find $\mathbf{u}(\mathbf{x})$ such that

$$\int_\Omega \varepsilon(\mathbf{v}) : \sigma(\mathbf{u}) d\Omega = \int_\Omega \mathbf{b} \cdot \mathbf{v}\, d\Omega + \int_{\Gamma_N} \hat{\mathbf{t}} \cdot \mathbf{v}\, ds \tag{4}$$

for every admissible displacement field $\mathbf{v}(\mathbf{x})$. In order for the natural element approximation using a given natural element grid $\Im_{NEM}$ composed of N nodes shown in Fig. 2(a), and trial and test displacement fields $\mathbf{u}(\mathbf{x})$ and $\mathbf{v}(\mathbf{x})$ are expanded as

$$\mathbf{u}_h(\mathbf{x}) = \sum_{J=1}^{N} \mathbf{u}_J \varphi_J(\mathbf{x}) = \Phi \overline{\mathbf{u}} , \quad \mathbf{v}_h(\mathbf{x}) = \sum_{I=1}^{N} \mathbf{v}_I \psi_I(\mathbf{x}) = \Psi \overline{\mathbf{v}} \tag{5}$$

with Laplace interpolation functions $\varphi_J(\mathbf{x})$ and $\psi_I(\mathbf{x})$ shown in Fig. 2(b). As is well known, the approximation is classified into Buvnov-Galerkin and Petrov-Galerkin depending on whether the both basis functions are the same or not. In addition, Φ and Ψ are $(2 \times 2N)$ matrices containing N

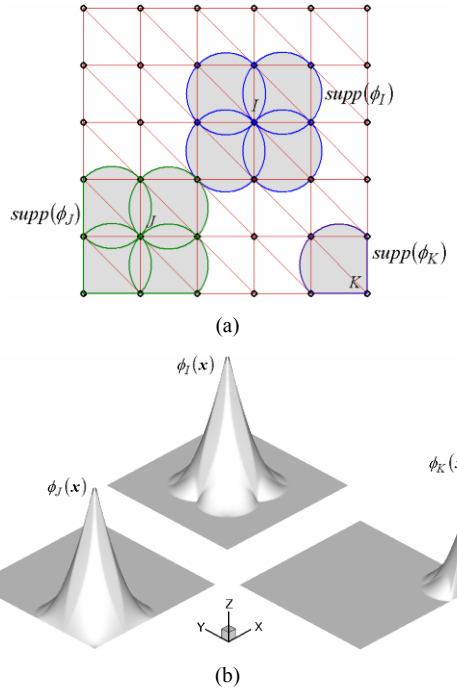

Fig. 2. Laplace interpolation functions [15]: (a) Supports; (b) shapes.

trial and test basis functions φ_J and ψ_I and $\bar{\mathbf{u}}$ and $\bar{\mathbf{v}}$ denote the $(2N\times 1)$ nodal vectors, respectively.

Introducing Eq. (5) into Eq. (4) leads to

$$\sum_{I}^{N}\mathbf{K}_I\bar{\mathbf{u}}=\sum_{I}^{N}\mathbf{F}_I \tag{6}$$

with the node-wise matrices $\mathbf{K}_I$ and vectors $\mathbf{F}_I$ defined by

$$\mathbf{K}_I=\int_{\Omega_v^I}(\mathbf{L}\Psi)^T\,\mathbf{E}(\mathbf{L}\Phi)\,d\Omega \tag{7}$$

$$\mathbf{F}_I=\int_{\Omega_v^I}\Psi^T\mathbf{b}\,d\Omega+\int_{\Gamma_N\cap\Omega_v^I}\Psi^T\hat{\mathbf{t}}\,ds \tag{8}$$

where $\mathbf{L}$ is the (3×2) divergence-like operator defining Cauchy strain tensor and $\mathbf{E}$ indicates the (3×3) material constant matrix of linear elasticity. The numerical integration in natural element method is carried out over the supports $\Omega_v^I=supp(\psi_1(\mathbf{x}))$ of each test basis function.

The numerical integration for calculating $\mathbf{K}_I$ and $\mathbf{F}_I$ in most meshfree methods is made by applying the conventional Gauss quadrature rule to the extra background mesh. It is also performed by the Gauss quadrature rule in the natural element method, but the additional effort to construct a background mesh is not needed any more because Delaunay triangles generated in the process for defining the Laplace interpolation functions serve as a background mesh. However, the numerical integration accuracy in the natural element method is influenced by the type of test basis functions. Differing from the Buvnov-Galerkin natural element (BG-NE) method in which Laplace interpolation functions $\varphi_J(\mathbf{x})$ are used for both the test and trial functions, the Petrov-Galerkin natural element (PG-NE) method in the current study uses the 3-node triangle-based Constant-strain finite element (CS-FE) basis functions $\psi_J(\mathbf{x})$ for the test functions. Figs. 3(a) and (b) comparatively represent the supports of trial and test basis functions and their intersection Ω_{IJ}^{int} in BG- and PG-NE methods, respectively.

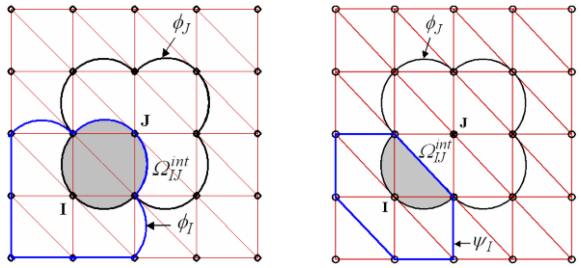

Fig. 3. Intersection Ω_{IJ}^{int} between trial function and test function [15]: (a) φ_I and φ_J in BG-NEM; (b) ψ_I and φ_J in PG-NEM.

In case of BG-NE method, neither the support of φ_I nor the intersection Ω_{int}^{IJ} between φ_I and φ_J does not coincide with a union of Delaunay triangles within $supp(\varphi_1)$ to which the regular Gauss quadrature rule is applied. Thus, one encounters the numerical difficulty in calculating $\mathbf{K}^I$ and $\mathbf{F}^I$, because the numerical integration accuracy and the convergence rate of the Gauss quadrature rule deteriorates if the support of integrand function does not coincide with a regular integration region in background mesh, as pointed out in a book by Strang and Fix [22]. Differing from the BG-NE method, the support $supp(\psi_1)$ of test basis function in the PG-NE method is composed of a union of Delaunay triangles, so that the discrepancy between the regular Gauss integration domain and the test function support does not occur any more. Furthermore, the intersection region Ω_{IJ}^{int} between the CS-FE basis function ψ_I and Laplace basis function φ_J is always contained within the support $supp(\psi_1)$ of the trial basis function ψ_I.

3. Stress recovery techniques

In order to explore the recovery characteristics of stresses which are approximated by the natural element method, two representative stress recovery techniques using Laplace interpolation functions are employed, the global L_2-projection method [2] and the local patch recovery technique (SPR) [3]. For the comparison purpose, the local patch recovery is also performed using the Lagrange-type basis functions used for 3- and 6-node triangular elements. In case of the finite element approximation, it is well known that the direct differentiation of approximate solution $\mathbf{u}_h$ leads to inaccurate non-smooth strain and stress fields. Furthermore, by virtue of the weighted residual method, the approximate solution $\mathbf{u}_h$ shows the super-convergence in $\mathbf{u}_h'$ at Gauss integration points. The basic motivation of these stress recovery techniques is to interpolate the enhanced stress field $\hat{\sigma}(\mathbf{x})$ which can minimize the difference between σ_h and $\hat{\sigma}$ in the L_2-norm sense,

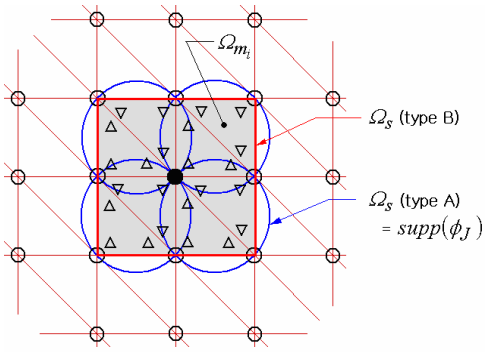

(a)

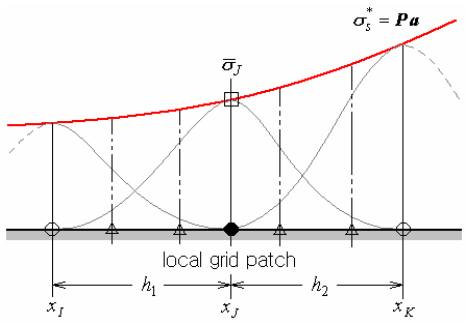

(b)

Fig. 4. (a) A local patch Ω_s for node J; △ Gauss points; ● nodal values determined by recovery procedure; ○ patch assembly points; (b) locally recovered stress.

either over the entire domain Ω or within each element patch Ω_s. Based upon the super-convergence characteristic of finite element approximation, the stress recovery by these techniques is numerically implemented using the same Gauss integration points which are used to obtain the approximate solution $\mathbf{u}_h$.

We first consider the stress recovery by the local patch recovery technique, for which two types of local grid patches are considered. Referring to Fig. 4(a), a local grid patch Ω_s for node J in NEM grid is defined either by $supp(\varphi_J)$ in type A or by

$$\Omega_s = \cup_{i=1}^{m} \Omega_{m_i}, \quad \Omega_{m_i} \subset supp(\varphi_J) \tag{9}$$

in type B with a total of m_m Delaunay triangles within the support of φ_J. Referring to Fig. 4(b), the stress field $\sigma_s^*(\mathbf{x})$ to be recovered within the local grid patch Ω_s is interpolated by

$$\sigma_s^* = \mathbf{Pa}, \quad \mathbf{P} = \left[\varphi_{\mathbf{m}_1}, \varphi_{m_2}, \cdots, \varphi_{m_n}\right] \tag{10}$$

with $\mathbf{a}$ being a set of unknown parameters and a total of m_n Laplace interpolation functions which have non-vanishing values within a local grid patch Ω_s. As shown in Fig. 4(a), the total number m_n is greater than the total number m_m. Then, the recovered enhanced stress filed could be obtained by minimizing

$$F(\mathbf{a}) = \int_{\Omega_s} \left(\sigma_h - \sigma_s^*\right)^2 dA. \tag{11}$$

Substituting Eq. (10) into Eq. (11) leads to

$$\hat{\mathbf{K}}\mathbf{a} = \hat{\mathbf{F}} \tag{12}$$

with the local stiffness matrix $\hat{\mathbf{K}}$ and the local load vector $\hat{\mathbf{F}}$ defined by

$$\hat{\mathbf{K}} = \int_{\Omega_s} \mathbf{P}^T\mathbf{P}\, dA, \quad \hat{\mathbf{F}} = \int_{\Omega_s} \mathbf{P}^T\sigma_h dA. \tag{13}$$

The local patch recovery is carried out node by node within a NEM grid until the nodal recovered stresses are completely determined in sequence.

Meanwhile, in the global stress recovery, individual local patches Ω_s are extended to the whole problem domain Ω and the recovered stress field $\sigma_s^*(\mathbf{x})$ is interpolated with all the Laplace interpolation functions in a NEM grid. In other words, a set $\mathbf{P}$ of interpolation functions in Eq. (10) and the residual functional $F(\mathbf{a})$ in Eq. (11) become as follows:

$$\mathbf{P} = \left[\varphi_1, \varphi_2, \cdots, \varphi_{N_n}\right], \qquad F(\mathbf{a}) = \int_{\Omega} \left(\sigma_h - \sigma_s^*\right)^2 dA. \tag{14}$$

Thus, the global stress recovery ends up with an extended matrix system of simultaneous Eq. (11) to compute a set $\mathbf{a}$ of nodal parameters defined by

$$\mathbf{a}^T = \left\{\left(\hat{\sigma}_{xx}, \hat{\sigma}_{yy}, \hat{\sigma}_{xy}\right)_1, \left(\hat{\sigma}_{xx}, \hat{\sigma}_{yy}, \hat{\sigma}_{xy}\right)_2, \cdots, \left(\hat{\sigma}_{xx}, \hat{\sigma}_{yy}, \hat{\sigma}_{xy}\right)_N\right\} \tag{15}$$

as Eq. (6) for computing the nodal displacement vector $\overline{\mathbf{u}}$.

Next, Fig. 5 represents the element patches for linear and quadratic triangular elements when Lagrange-type basis functions, instead of Laplace interpolation functions, are used for the local stress recovery. Except for replacing Laplace interpolation function with Lagrange-type basis function, theses element patches are identical with the type B of local grid patches shown in Fig. 4(a). In case of linear element patches, only the interior nodal values are determined for each element patch, as in the local patch recovery using Laplace interpolation functions. Meanwhile, in case of quadratic element patches, the nodal values of the internal side nodes as well as an internal vertex node are determined at each patch recovery computation. Since the nodal values of side nodes could be calculated more than once, two options would be considered to determine their values. One is to update their values along with the patch recovery, the other is to take the averaged values. In the current study, the former option is taken to determine the nodal values of side nodes. The strains are also recovered in the same manner, and the recovered stress and

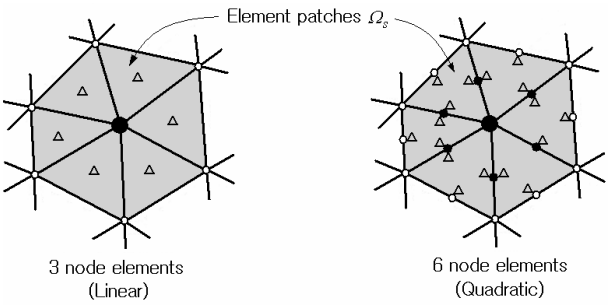

Fig. 5. Element patches for linear and quadratic triangular elements (Zienkiewicz and Zhu, 1992); △ Gauss points; ● nodal values determined by recovery procedure; O patch assembly points.

strains field over the problem domain are interpolated using either Laplace interpolation functions or Lagrange-type finite element basis functions.

In the current study, the accuracy of recovered strain and stress fields is estimated in terms of the energy-norm error defined by

$$\left\|\hat{\mathbf{u}}-\mathbf{u}_{ref}\right\|^2_{E(\Omega)}=\int_{\Omega}\left(\hat{\varepsilon}-\varepsilon_{ref}\right)\cdot\left(\hat{\sigma}-\sigma_{ref}\right)dA \tag{16}$$

with $\left(\cdot\right)_{ref}$ being the analytic solutions. The recovered strain $\hat{\varepsilon}$ is also obtained by the same recovery procedure as for the stress. The calibration of this absolute error by the total strain energy $U\left(\mathbf{u}_{ref}\right)$ leads to the global relative error defined by

$$\xi_G=\left\|\hat{\mathbf{u}}-\mathbf{u}_{ref}\right\|_{E(\Omega)}/\left|2U\left(\mathbf{u}_{\mathbf{ref}}\right)\right|^{1/2}=\left\|\hat{\mathbf{u}}-\mathbf{u}_{ref}\right\|_{E(\Omega)}/\left\|\mathbf{u}_{ref}\right\|_{E(\Omega)}. \tag{17}$$

4. Numerical experiments

Two numerical examples are taken to compare the stress recovery techniques considered in this study, in terms of the stress distributions before and after stress recovery and the global errors of recovered stresses with respect to the exact analytical ones. Two kinds of NEM grids, uniform and locally refined, are constructed and 13 Gauss integration points are used for both the natural element approximation and the stress recovery.

Fig. 6(a) represents a revisited plane strain plate problem with an internal circular hole under uniform unidirectional tension, where a darkened quarter at the right upper is taken for the numerical simulation from the problem symmetry. The reader may refer to a book by Timoshenko and Goodier [23] for the exact analytic solution for $t_x=1.0Pa$. The width b and the hole diameter $2a$ are taken by $10.0\,m$ and $1.0\,m$, respectively. Fig. 6(b) shows a locally refined NEM grid generated with the total of 1537 nodes, where the local region along the hole boundary is refined to effectively capture the stress singularity stemming from the boundary layer effect [24]. In the narrow thin region along the boundary of thin elastic structure, the strains and stresses exponentially grow up in the normal direction towards the boundary.

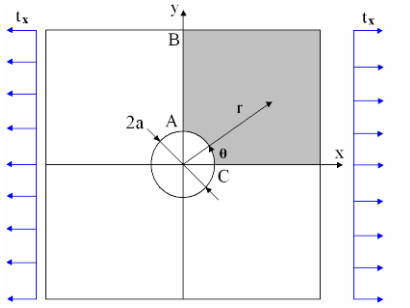

(a)

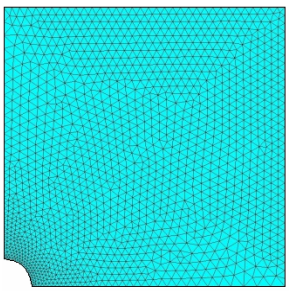

(b)

Fig. 6. (a) Plate with a circular hole subject to unidirectional tension (plane strain condition); (b) locally refined non-uniform NEM grid ($N=1537$).

The problem was solved by the PG-NE method and the stresses were recovered by the global and local recovery techniques using Laplace interpolation functions. The local stress recovery was basically carried out using the type A of local grid patches. The distributions of stress σ_{xx} along the vertical line A-B are comparatively represented in Fig. 7(a), where those of the analytic solution and bare stress are also included for the comparison purpose. Here, the term bare is used to indicate the stresses that were directly calculated from the approximate solution $\mathbf{u}_h$ without the stress recovery. It is observed that both the bare and the globally recovered stresses are in good agreement with the exact solution, but the local stress recovery shows the remarkable discrepancy near two end points A and B. These features of three methods can be also observed from Fig. 7(b) representing the effective stress distributions along the circular path C-A. The local stress recovery is shown to be in a good agreement with the analytic solution like the global stress recovery, but it produces the remarkable discrepancy at both ends C and A. Meanwhile, one can see the slight fluctuation through a whole range of the bare effective stress distribution. It has been observed that these features remain the same when the grid density is increased.

The stress distributions obtained by the local stress recovery techniques using the patch type B are comparatively represented in Fig. 8, where 3- and 6-node indicate that the stress recovery was made by the Lagrange-type finite element basis functions. First, it is found for the Laplace interpolation function that the patch type A shows a slightly more accurate dis-

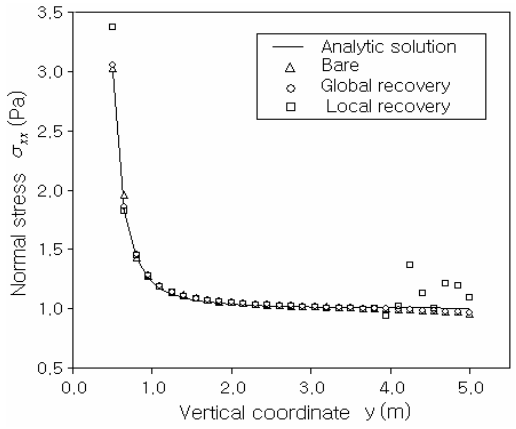

(a)

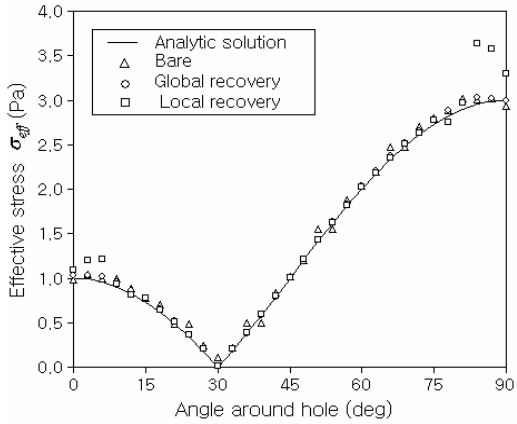

(b)

Fig. 7. Comparison of stress distributions for locally refined NEM grid ($N = 1537$): (a) Normal stress σ_{xx} along the vertical line A-B; (b) effective stress along the circular path C-A.

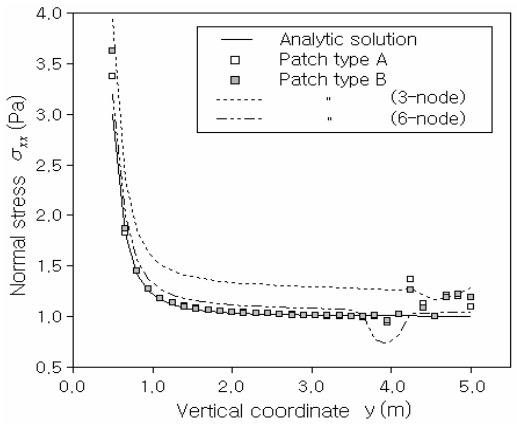

(a)

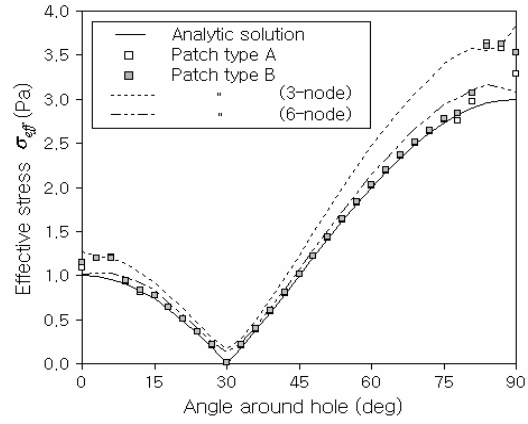

(b)

Fig. 8. Comparison between patch types A and B (locally refined NEM grid with $N = 1537$): (a) Normal stress σ_{xx} along the vertical line A-B; (b) effective stress along the circular path C-A.

tribution than type B, but the improvement is shown to be insignificant. In case of Lagrange-type FE basis functions, the 3-node linear function leads to the stress distributions much higher than all the other cases including the exact analytic solution. It is because the constant-strain finite element basis functions are not smooth enough to appropriately interpolate the bare stress approximated by Laplace interpolation functions. The big difference in the stress distributions becomes significantly smaller when the 6-node quadratic basis functions are used, but nevertheless a big discrepancy still remains in a local region.

Next, a rectangular plate shown in Fig. 9(a) with symmetric edge cracks is considered, which is in the plane strain state and subject to uniform vertical distributed load σ_∞. This problem was tested by Tracey [25] and later studied by Barsoum [26] using singular quadratic iso-parametric finite elements, and the stress distributions along the circular path Γ near the crack tip are concerned for the current study. The relative radius of Γ is set by $r/a = 0.0139$ and the material properties are the same as the previous example. A darkened quarter is taken for the natural element analysis from the

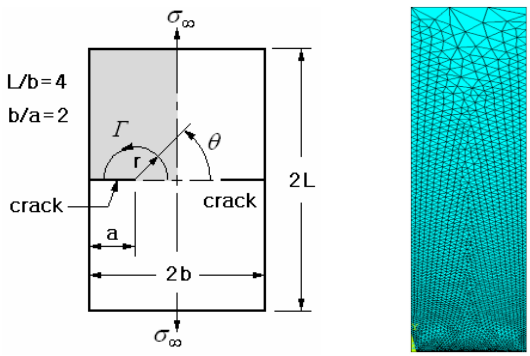

(a) (b)

Fig. 9. (a) A plane strain rectangular plate with symmetric edge cracks; (b) a gradient NEM grid ($N = 2516$).

symmetry of problem, and a gradient NEM grid having the highest grid density at the crack tip is used as shown in Fig. 9(b) to capture the $1/\sqrt{r}$ stress singularity near the crack tip as accurate as possible. The stress intensity factor for this type of problem is expressed by (with the correction factor C of 1.02 (ASTM [27]),

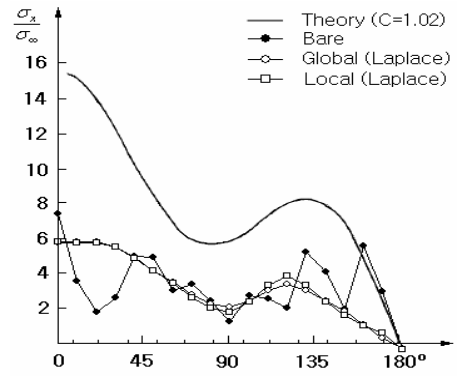

(a)

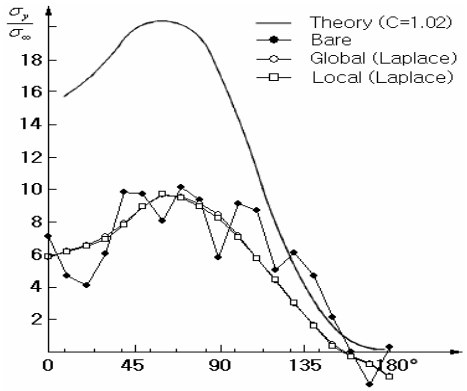

(b)

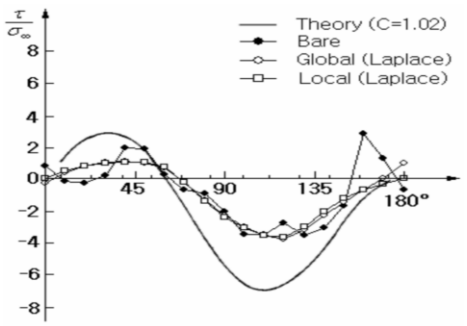

(c)

Fig. 10. Comparison of stress distributions along the circular path $(r/a=0.0139)$: (a) σ_{xx}; (b) σ_{yy}; (c) τ_{xy}.

$$K_I = \sigma_\infty (\pi a)^{\frac{1}{2}} \left(\frac{2b}{\pi a} \tan \frac{\pi a}{2b} \right) \cdot C. \tag{18}$$

The problem was solved by the PG-NE method using 13 Gauss integration points and the recovered stresses were obtained by both the global and local recovery techniques using the Laplace interpolation functions. The stress distributions along the circular path Γ near the crack tip are comparatively represented in Fig. 10. First of all, it is found that the present gradient NEM grid used for the crack analysis provides the stress level lower than the exact value, but the recovered stresses show the distributions similar to the exact ones. But, it is observed that the bare stresses lead to the significant fluctuation in their distributions, which is contrary to the stress distributions shown in Fig. 7 along the boundary of internal hole and the vertical line in the previous example. It is noted that the paths taken in the previous example are placed on the edges of fine Delaunay triangles but the circular path in the current example traverse the coarse Delaunay triangles. Differing from the bare stresses, the recovered stresses lead to the smoothened distributions and no remarkable difference is observed between the global and local recovery techniques. From the comparison of stress distributions through two examples, it has been observed that the bare stresses provide the accurate and smooth distributions only when the path is placed on the edge of fine Delaunay triangles. Both the global and local recovery techniques using Laplace interpolation functions provide the improved smoothened stress distributions, except for the occurrence of remarkable discrepancy near the end points of path in the local recovery technique. Meanwhile, the local recovery techniques using Lagrange-type FE basis functions lead to the stress distributions showing both the remarkable discrepancy and the local fluctuation.

Next, the parametric experiments with respect to the total number N of grid points were performed, in order to compare the convergence rates in the global error sense for the stress recovery techniques. The parametric experiments were carried out by the PG-NE method using the previous plate problem with an internal circular hole shown in Fig. 6(a). Uniform and locally refined NEM grids are used and the locally refined ones are generated by increasing the grid density in the vicinity of the internal hose, as illustrated in Fig. 6(b). The total numbers of grid points which are set for the parametric experiments are as follows: 131, 371, 736, 1338 and 2312 for the uniform grids, and 56, 204, 427, 1537 and 2668 for the locally refined grids. The convergence rates of the global relative energy-norm errors Eq. (17) in log-log scale are comparative represented in Fig. 11. As shown in Fig. 11(a) for uniform NEM grids, the global and local recovery techniques using Laplace interpolation functions show almost the same convergence rates as the bare stress, but 3- and 6-node finite element basis functions exhibit lower convergence rates. Meanwhile, for the locally refined NEM grids shown in Fig. 11(b), the convergence rates of the bare stress and the global recovery technique using Laplace interpolation functions are much higher at course grids, but those are observed to be slow down with the increase of grid density. Meanwhile, the remaining three local recovery techniques provide almost the uniform convergence rates which are slightly higher than those of uniform NEM grids. Thus, it is confirmed that the bare stresses approximated directly by the PG-NE method provide the convergence rates higher than those of the local recovery techniques, in particular at locally refined NEM grids. In addition, the convergence rates are improved only by the global stress recovery using Laplace interpolation functions even though the improvement is not remarkable.

The global relative errors and the convergence rates were

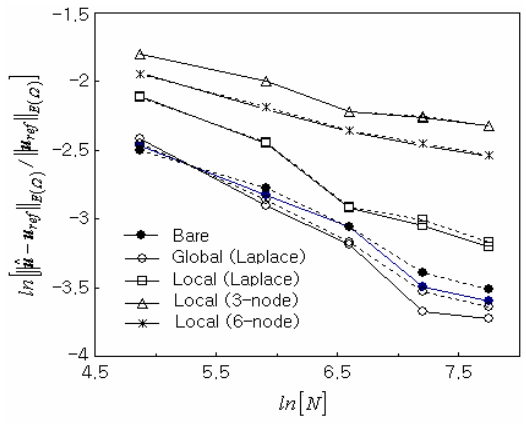

(a)

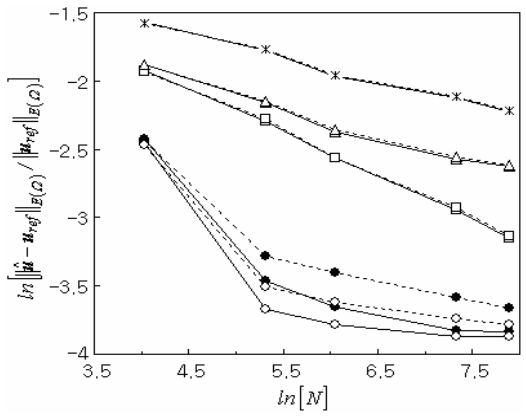

(b)

Fig. 11. Comparison of the convergence rates (─ PG-NEM, --- BG-NEM; ● bare, ○ global (Laplace), □ local (Laplace), △ local (3-node), ✳ local (6-node)): (a) Uniform grid; (b) locally refined grid.

also evaluated for the BG-NE method in which Laplace interpolation functions, instead of Lagrange-type finite element basis functions, are used for the test basis functions. The comparison of the global relative errors between PG-NE and BG-NE methods is also represented in Fig. 11 for uniform and locally refined NEM grids. It is observed that the global relative errors of BG-NE method are as a whole larger than those of PG-NE method for both uniform and locally refined NEM grids. The relative differences are apparent at the bare stress and the global stress recovery, while those at three local recovery techniques are negligible. As represented in our previous paper [15], together with the discussion on two NEM methods in Sec. 3, the approximation accuracy of the BG-NE method deteriorates owing to the numerical integration inaccuracy. Thus, both the bare stresses and the global stress recovery of the BG-NE method produce the apparently larger errors. But, such numerical accuracy deterioration does not apparent at three local stress recovery techniques, because the error contribution by the numerical integration inaccuracy in the BG-NE method is relatively smaller than one caused during the process of local stress recovery.

5. Conclusions

The stress recovery for the natural element method in 2-D solid mechanics has been addressed in this paper, in order to explore whether and how much the bare stresses could be improved by the stress recovery. The global and local stress recovery approaches based on the L_2-projection method were considered, in which the recovered stress field was basically interpolated by Laplace interpolation functions. Here, for the local stress recovery, two types of element patches were considered and Lagrange-type finite element basis functions were additionally employed to interpolate the recovered stress field. The characteristics of the stress recovery techniques were investigated in terms of the stress distributions and the global energy-norm errors, with respect to the type of NEM grid and the total number of grid points.

From the comparison of stress distributions along the specific paths in two representative examples, a plate with an internal circular hole and a rectangular plate with symmetric edge cracks, the following main observations were made: The bare stresses approximated by the natural element method provide the acceptable and smooth distributions only when the path is placed on the edges of fine Delaunay triangles, if not those produce the significantly fluctuating stress distributions. Meanwhile, both the global and local stress recovery techniques using Laplace interpolation functions lead to the improved smoothened stress distributions, except for the occurrence of remarkable discrepancy near the end points of path in the local recovery technique. In the local stress recovery using Laplace interpolation functions, the patch type A shows a slightly better distribution than type B, but the improvement is not remarkable. On the other hand, the local stress recovery techniques using Lagrange-type FE basis functions seem inappropriate for the natural element method because those lead to less accurate and locally fluctuating stress distributions.

From the comparison of the global relative errors, it has been observed that the convergence rates of the bare stress c ould be improved only by the global stress recovery using Laplace interpolation functions. The local recovery techniques show the convergence rates worse than the bare stress, for both uniform and locally refined NEM grids. It has been also observed, from the comparison of two natural element methods, that the global relative errors of the BG-NE method are as a whole larger than those of the PG-NE method, owing to the inherent numerical integration inaccuracy in the BG-NE method.

The current study is limited to 2-D linear elasticity, but it could be extended to 3-D problems with thin domain, such as plate- and shell-like structures, by introducing the assumed displacement field in the thickness direction. It would be worthwhile, and which represents a topic that deserves future work.

Acknowledgment

This work was supported by the Hongik University new faculty research support fund.

References

[1] D. S. Burnett, *Finite Element Analysis*, Addison-Wesley Publishing Company, New York, USA (1987).

[2] H. J. Brauchli and J. T. Oden, On the calculation of consistent stress distributions in finite element applications, *International Journal for Numerical Methods in Engineering*, 3 (1971) 317-325.

[3] O. C. Zienkiewicz and J. Z. Zhu, The superconvergent patch recovery and a posteriori error estimates. Part 1: The recovery technique, *International Journal for Numerical Methods in Engineering*, 33 (1992) 1331-1364.

[4] T. Blacker and T. Belytschko, Superconvergent patch recovery with equilibrium and conjoint interpolant enhancements, *International Journal for Numerical Methods in Engineering*, 37 (1994) 517-536.

[5] B. Boroomand and O. C. Zienkiewicz, Recovery by equilibrium, *International Journal for Numerical Methods in Engineering*, 40 (1997) 137-164.

[6] T. Belytschko, Y. Y. Lu and L. Gu, Element-free Galerkin methods, *International Journal for Numerical Methods in Engineering*, 37 (1994) 229-256.

[7] W. K. Liu, S. Jun and Y. F. Zhang, Reproducing kernel particle methods, *International Journal for Numerical Methods in Fluids*, 20 (1995) 1081-1106.

[8] C. A. Duarte and J. T. Oden, An h-p adaptive method using clouds, *Computer Methods in Applied Mechanics and Engineering*, 139 (1996) 237-262.

[9] J. M. Melenk and I. Babuska, The partition of unit finite element method: basic theory and applications, *Computer Methods in Applied Mechanics and Engineering*, 139 (1996) 289-314.

[10] S. N. Atluri and T. Zhu, A new meshless local Petrov-Galerkin (MLPG) approach in computational mechanics, *Computational Mechanics*, 22 (1998) 117-127.

[11] J. Braun and M. Sambridge, A numerical method for solving partial differential equations on highly irregular evolving grids, *Nature*, 376 (1995) 655-660.

[12] N. Sukumar and B. Moran, C^1 natural neighbor interpolant for partial differential equations, *Numerical Methods in Partial Differential Equations*, 15 (1999) 417-447.

[13] M. Sambridge, J. Braun and H. McGueen, Geophysical parameterization and interpolant of irregular data using natural neighbors, *Geophysical Journal International*, 122 (1995) 837-857.

[14] N. Sukumar, A. Moran and T. Belytschko, The natural element method in solid mechanics, *International Journal for Numerical Methods in Engineering*, 43 (1998) 839-887.

[15] J. R. Cho and H. W. Lee, A Petrov-Galerkin natural element method securing the numerical integration accuracy, *Journal of Mechanical Science and Technology*, 20 (1) (2006) 94-109.

[16] B. Calvo, M. A. Martinez and M. Doblaré, On solving large strain hyperelastic problems with the natural element method, *International Journal for Numerical Methods in Engineering*, 62 (2) (2005) 159-185.

[17] J. R. Cho and H. W. Lee, 2-D large deformation analysis of nearly incompressible body by natural element method, *Computers and Structures*, 84 (2006) 293-304.

[18] J. R. Cho and H. W. Lee, 2-D frictionless dynamic contact analysis of large deformable bodies by Petrov-Galerkin natural element method, *Computers and Structures*, 85 (2006) 1230-1242.

[19] Y. Zhang, H. L. Yi and H. P. Tan, Natural element method for heat transfer in two-dimensional semitransparent medium, *International Journal of Heat and Mass Transfer*, 56 (1-2) (2013) 411-423.

[20] J. R. Cho and H. W. Lee, Calculation of stress intensity factors in 2-D linear fracture mechanics by Petrov-Galerkin natural element method, *International Journal for Numerical Methods in Engineering*, 98 (2014) 819-839.

[21] J. R. Cho, H. W. Lee and W. S. Yoo, Natural element approximation of Reissner-Mindlin plate for locking-free numerical analysis of plate-like thin elastic structures, *Computer Methods in Applied Mechanics and Engineering*, 256 (2013) 17-28.

[22] F. Strang and G. J. Fix, *An Analysis of the Finite Element Method*, Prentice-Hall, New Jersey (1973).

[23] S. P. Timoshenko and J. N. Goodier, *Theory of Elasticity*, McGraw-Hill, New York (1970).

[24] J. R. Cho and J. T. Oden, Locking and boundary layer in hierarchical models for thin elastic structures, *Computer Methods in Applied Mechanics and Engineering*, 149 (1997) 33-48.

[25] D. M. Tracey, Finite elements for determination of crack tip elastic stress intensity factors, *Engineering Fracture Mechanics*, 3 (1971) 255-265.

[26] R. S. Barsoum, On the use of isoparametric finite elements in linear fracture mechanics, *International Journal for Numerical Methods in Engineering*, 10 (1976) 25-37.

[27] Fracture *Toughness Testing and Its Applications*, ASTM Spec. Tech. Pub., 381 (1965) 43-51.

Jin-Rae Cho received his B.S. degree in Aeronautical Engineering from Seoul National University in 1983. He then received his M.S. and Ph.D. degrees from The University of Texas at Austin in 1993 and 1995, respectively. He is currently an Associate Professor at the Department of Naval Architecture and Ocean Engineering in Hongik University. His major research field is the computational mechanics in solid/structural /bio mechanics, ocean engineering and materials science.